

Effect of Mg Content on the Structure, Properties and Cytotoxicity of Biodegradable Zn-Fe-Mg Alloys

E.D. Abdrakhmanova^{1,2,*} , E.D. Khafizova¹ , M.V. Polenok¹ , R.K. Islamgaliev¹ ,
Zhen Li² , Li Li² , Yingru Liang² , Meng Zhang² 

¹ Ufa University of Science and Technology, Zaki Validi Str., 32, Ufa, 450076, Russia
² Harbin Engineering University, Nantong Str, No. 145, Harbin Heilongjiang, 150001, China

Article history

Received April 11, 2025
Accepted April 19, 2025
Available online April 20, 2025

Abstract

Interest in biodegradable materials for temporary implants based on zinc alloys has been growing annually. The Zn-Fe-Mg alloys are of special interest, as each of its constituent elements is independently considered as biodegradable metallic material. This study presents a comprehensive investigation of the Zn-1%Fe-1%Mg and Zn-1%Fe-5%Mg alloys subjected to high-pressure torsion. A comparative analysis was conducted on the microstructure of the alloys in both as-cast and deformed states, highlighting differences in their phase composition, strength and cytotoxicity. When the magnesium content exceeds 3 wt.%, an additional phase ($MgZn_{11}$) precipitates alongside the existing Mg_2Zn_{11} phase. Deformation processing of the Zn-1%Fe-1%Mg alloy effectively reduces its brittleness and promotes a more homogeneous distribution of the Mg_2Zn_{11} eutectic throughout the sample volume. In contrast, the Zn-1%Fe-5%Mg alloy retains excessive brittleness even after deformation. The addition of magnesium was found also to accelerate corrosion rates. Nevertheless, the strength, corrosion, and cytotoxicity properties of the Zn-1%Fe-1%Mg alloy meet the requirements for biodegradable materials.

Keywords: Zn; Biodegradable materials; Corrosion; High pressure torsion; Cytotoxicity

1. INTRODUCTION

The annual incidence of traumatic injuries involving complex bone fractures and soft tissue tears continues to rise. Those injuries require surgical intervention with the use of temporary implants [1,2]. Nowadays the application materials for the implants are made of titanium and cobalt-chromium, which can cause serious complications during exploitation, for example the inflammation of the adjacent tissues [3]. A significant problem of implants is the migration of toxic ions into ambient tissues. It has occurred through interaction of implant's metal with an active aggressive liquid of human organism. Thus, electrolytes of living organisms induce the biocorrosion of metals; as a result, particles penetrate adjacent tissues and bloodstream. The released metal ions do not always bind with biomolecules; instead, reactive ions may combine with

water or anions to form oxides, hydroxides, or inorganic salts. These compounds can cause cytotoxicity, allergic reactions or other negative biological effects. Consequently, the necessity in manufacturing implants which do not cause an inflammation response while inside human body for an extended period and accelerating the recovery of patients is increasing.

Biodegradable implants due to gradual dissolution do not cause the inflammation during prolonged residence in the body and simultaneously create favorable conditions for accelerated bone formation—osteogenesis [4–6]. Alloys based on zinc have the most suitable corrosion rates [7], but pure zinc is a brittle material and exhibits insufficient mechanical properties. However, it is known that the number of favorably oriented planes increase after grain refinement and the multiple sliding is activated. The samples of a pure zinc processed by high pressure torsion (HPT) were

* Corresponding author: E.D. Abdrakhmanova, e-mail: elmira.abdr2019@mail.ru

studied in Ref. [8]. It has been stated that for the as-cast samples the values of microhardness were 38 HV, ultimate tensile strength (UTS) was 75 MPa; for the sample deformed by 10 turns of HPT the microhardness was 41 HV and the UTS was 130 MPa [8].

Alloying represents another effective approach for strength enhancement of pure zinc through both solid solution strengthening and second-phase precipitation mechanisms.

Zinc alloy of the Zn-Fe-Mg system is of special interest since each constituent element independently is considered as biodegradable metallic material [9]. In research [10] the Zn-xMg alloys ($x = 0.5\%$, 0.8% , 1%) were studied and it was demonstrated that Zn-0.8%Mg after extrusion exhibits the highest UTS of 214 MPa with the elongation of 20%.

With the increase in magnesium content there is an enhancement in the volume fraction of eutectic mixture Zn + Mg₂Zn₁₁ contributing to the formation of smaller grains in the as-cast state. The Zn-0.02%Mg, Zn-0.05%Mg and Zn-0.2%Mg alloys after hot extrusion, cold rolling and annealing have been investigated in Ref. [11]. With the increase in magnesium content the average grain size decreased; for Zn-0.02%Mg and Zn-0.2%Mg it was 60 and 20 microns, respectively. UTS and yield strength were enhanced by grain refinement and second phase strengthening mechanisms. Moreover, during the corrosion tests in Hanks solution a positive correlation was shown between corrosion rates and magnesium content in the alloy.

Thus, the common tendency of decrease in ductility and increase in strength of the Zn-xMg alloys is observed. However, when certain magnesium content is reached in the composition, the embrittlement appears. Consequently, enhancing of strength will be achieved by combining the optimal alloy composition and further grain refinement. In this paper, a comprehensive study of the properties of the Zn-1%Fe-1%Mg and Zn-1%Fe-5%Mg alloys subjected to HPT is presented.

2. MATERIALS AND METHODS

The research material consists of the Zn-1%Fe-1%Mg and Zn-1%Fe-5%Mg alloys. The casting was performed in a chamber furnace using a graphite crucible with a diameter of 20 mm, which had a lid, at a temperature of 580 °C. The cast samples were cooled in air. Subsequently, the samples were subjected to homogenizing annealing at a temperature of 350 °C for 12 hours. The chemical composition was determined by X-ray fluorescence spectroscopy on an ARL Optim'X X-ray spectrometer.

The disks with a diameter of 20 mm and a thickness of 1.8 mm were cut out of the annealed samples on the ARTA 120 CNC EDM. Consequently, the samples were subjected to HPT at room temperature with a pressure of 6 GPa. The

number of revolutions for the Zn-1%Fe-5%Mg alloy was 0.5, 1, 2, 3, 5, 6, 8, and 10, while for Zn-1%Fe-1%Mg alloy was 1, 3, 5, 6, and 10. The as-cast after homogenization annealing (further referred to as initial) and deformed samples were investigated.

Static tensile tests were performed on small samples (Fig. 1) at room temperature at a rate of 0.2 mm/min using the Instron 5982 electromechanical measuring system.

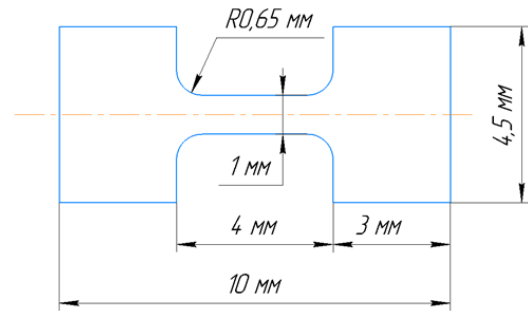


Fig. 1. Drawing of small samples for static tensile testing.

The microhardness of the deformed samples was measured on the hardness tester EMCO-Test DuraJet 10 using the Vickers method (GOST 9450–76) under a load of 0.1 kg and the exposure time under load of 10 seconds. The microhardness of the alloy was taken to be valued over 20 measuring points (in 1 mm increments over the entire diameter of the sample).

For the microstructure investigation, samples were preliminarily etched in a 15% H₂SO₄ solution. Microstructure and relief of corrosion surface studies were conducted on the scanning electronic microscope JEOL JSM-6490LV. EDS analysis of the sample's surface after corrosion tests and the pictures of microstructure of the initial samples were carried out on the scanning electronic microscope Tescan mira.

Corrosion tests were performed for 90 days in Ringer's solution (8.60 g/l NaCl, 0.30 g/l KCl, and 0.33 g/l CaCl₂, pH = 7.8) at a temperature of 38 °C. The method consisted of cleaning the corrosion products every 2 days, measuring weight, photo fixation, and further re-immersion in a new solution. Cleaning from corrosion products was carried out first in a solution of chromium VI oxide, then in distilled water using an ultrasonic bath to KAISI-105. After purification, the samples were dried and weighed on an EJ-123 electronic scale. The corrosion rate CR was calculated according to ASTM G3–63592 using the formula:

$$CR = \frac{87.6(M_0 - M_1)}{St\rho}, \quad (1)$$

where CR is corrosion rate (mm/year), S is sample surface area (cm²), M_0 is initial weight (mg), M_1 is weight after

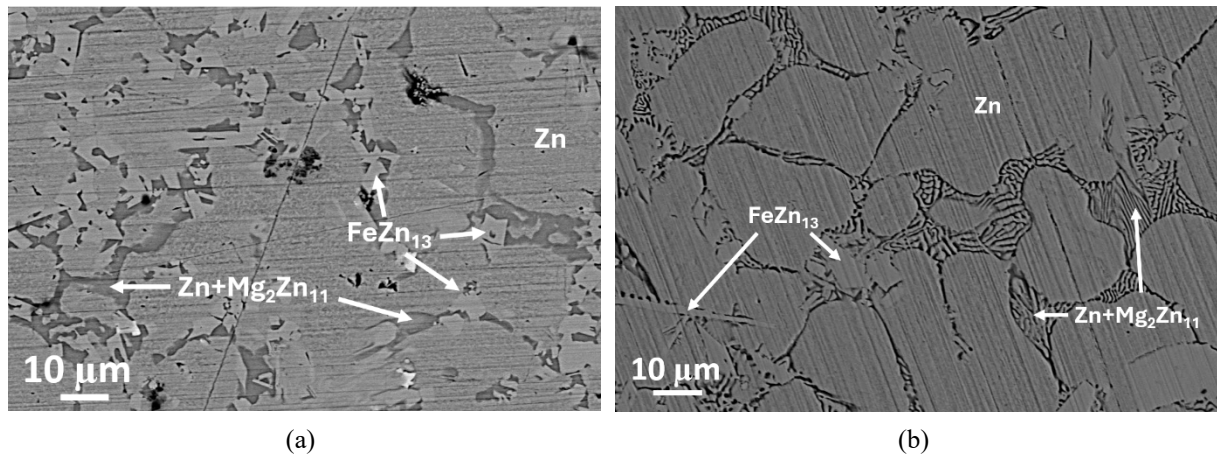


Fig. 2. Microstructure of initial samples: (a) Zn-1%Fe-1%Mg, (b) Zn-1%Fe-5%Mg; x 1000.

immersion (mg), t is exposure time (h), ρ is density of metal (g/cm^3).

A series of experiments were conducted to study the proliferative activity of MG63 cells in the presence of extracts of zinc alloy samples presented in the form of disks for 7 days. The viability evaluation of MG63 cells was carried out according to Ref. [12]. Morphological characteristics of the cells were investigated by using a fluorescence microscope Axio Observer with phase contrast and filter systems. After seven days of incubation, propidium iodide cell staining and microscopic analysis were conducted on samples of the alloy, using extracts at concentrations of 25% and 12.5%.

3. RESULTS AND DISCUSSION

3.1. Microstructure

Figure 2 presents the alloy structures of Zn-1%Fe-1%Mg (Fig. 2a) and Zn-1%Fe-5%Mg (Fig. 2b). In the initial state, the microstructure consists of three phases: zinc grains (Zn) with an average size of 35 microns, $\text{Mg}_2\text{Zn}_{11}$ eutectics that take place alongside the grain boundaries, and an intermetallic phase FeZn_{13} , represented by both small and large particles, which can reach 110 microns in length. With an increase in magnesium (Mg) content, the volume fraction of the $\text{Mg}_2\text{Zn}_{11}$ phase elevates, and it forms alternating areas with pure Zn (Fig. 2b). These sizes are conditioned by the phase diagram of Fe-Zn, according to which this phase solidifies sooner than others. During the cooling process, Fe precipitates from the zinc matrix, which leads to the formation of the FeZn_{13} phase [13].

The formation of these phases is confirmed by X-ray phase analysis [14,15]. In the Zn-1%Fe-5%Mg alloy, a FeZn_{11} phase was also detected. These data are in agreement with the study [16] on samples of Zn- x Fe ($x = 1\%$, 2%, 5%, 10%) alloys, where FeZn_{13} and FeZn_{11} are presented in each sample. According to the experimental

studies of the phase diagram of the Zn-Fe system, at a temperature of 417.4 °C, a eutectic reaction occurs, resulting in a structure consisting of ζ -phase (FeZn_{13}) and η (Zn, Fe) phase [17]. FeZn_{13} is presented by sharp dendritic crystals similar in form to a light-grey particles in Fig. 2.

According to phase diagrams, during the cooling of a Zn-Mg liquid containing 1 wt.% Mg to about 410 °C, the Zn solid solution crystallizes first. Then, at a temperature of 364 °C, an intermetallic compound $\text{Mg}_2\text{Zn}_{11}$ forms. Similar structures have been reported in research [18], where a Zn-1%Fe-5%Mg alloy exhibited equivalent hexagonal inclusions, which are conceivably Zn + MgZn_2 eutectics. Light-grey circles inside the hexagons contain less magnesium and are supposed to be the $\text{Mg}_2\text{Zn}_{11}$ phase, which formed on the surface of MgZn_2 . The presence of stable (Zn + $\text{Mg}_2\text{Zn}_{11}$) and metastable (Zn + MgZn_2) eutectics in a Zn-5%Mg alloy, layering on top of each other during the solidification process, has also been reported in other studies [19].

Application of HPT leads to changes in structure. In the Zn-1%Fe-1%Mg alloy, a band structure is formed by alternating phases of $\text{Mg}_2\text{Zn}_{11}$, Zn, and FeZn_{13} (Fig. 3a). HPT resulted in the crushing of the FeZn_{13} phase's grains, as well as a change in the shape and size of the particles. With an increase in the number of revolutions, i.e., the degree of deformation, not only the thinning of the band within the structure was observed but also further grain refinement in each phase [15]. On the other hand, in the Zn-1%Fe-5%Mg alloy, a fine-grained structure transformed into an ultrafine-grained. The average grain size was approximately 1 micron after 2 revolutions of HPT (Fig. 3b). The crushing of the solid Fe-Mg and FeZn_n phases occurred [14].

By applying a deformation, the $\text{Mg}_2\text{Zn}_{11}$ eutectics is refined and distributed in the direction of the deformation, a phenomenon that has also been observed after hot rolling of Zn-0.4%Mg and Zn-0.8%Mg alloys in the study [20]. The transition to an equilibrium state can be achieved through a series of metastable states, and the elevation of pressure

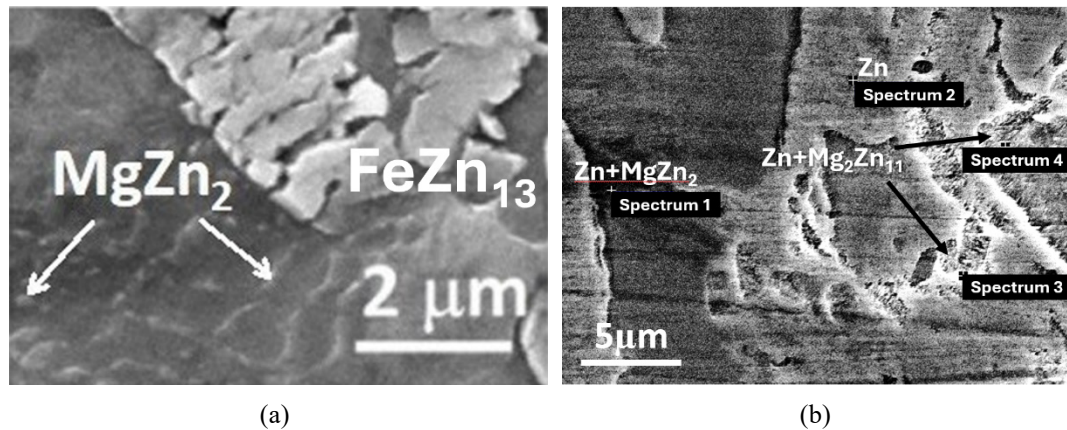


Fig. 3. Microstructure of the Zn-1%Fe-1%Mg (a) and Zn-1%Fe-5%Mg (b) alloys after HPT.

decreases the temperature of transition. Thus, when exposed to high hydrostatic pressures, there is an opportunity for a phase transition. In the Zn-1%Fe-1%Mg alloy, this phase transition occurs as follows: Zn (eutectics) + Mg_2Zn_{11} (eutectics) + $FeZn_{13}$ → Zn (phase) + Mg_2Zn_{11} (phase) + $MgZn_2$ (particles) + Zn (particles) [15].

3.2. Mechanical and corrosion properties

Mg enhances an alloy's strength through solid solution strengthening and dispersion strengthening with intermetallics particles. Thus, the microhardness of the Zn-1%Fe-1%Mg alloy is equal to 118 ± 5 HV [15] and the Zn-1%Fe-5%Mg alloy is 210 ± 4.6 HV [14].

However, the HPT treatment significantly affects the strength and ductility of a material. In the Zn-1%Fe-1%Mg alloy UTS reached 289 ± 11 MPa, and the elongation was up to $95 \pm 5\%$ in a highly deformed state [15]. High magnesium content can decrease the ductility because of the intermetallic phases brittleness, thereby all the Zn-1%Fe-5%Mg samples were destroyed in the elastic zone.

The presence of both Mg_2Zn_{11} and $FeZn_{13}$ explains the rise in brittleness as the rise of the volume fraction v_ζ of the $FeZn_{13}$ (ζ -phase) in the alloy leads to the appearance of sources of stress during deformation, where cracks form further. According to the formula (2):

The presence of both Mg_2Zn_{11} and $FeZn_{13}$ explains the rise in brittleness. The volume fraction v_ζ is found according to the following formula [22]:

$$v_\zeta = \frac{w_\zeta / \rho_\zeta}{w_\zeta / \rho_\zeta + (1 - w_\zeta) / \rho_{Zn}}, \quad (2)$$

where: $w_\zeta = x / 5.2$ is the weight fraction of $FeZn_{13}$ in the alloy, x is the content of the Fe component in the alloy (in wt.%), $\rho_\zeta = 7.32$ g/cm³ and $\rho_{Zn} = 7.14$ g/cm³ are the densities of $FeZn_{13}$ and Zn, respectively.

In our case, the 1 wt.% addition of Fe leads to the creation of $FeZn_{13}$, which makes up 18.8% of the volume fraction of the alloy. The formation of particles begins at a temperature of 530 °C, therefore during solidification, its size increases dramatically and can reach more than 350 microns in length [22]. The presence of coarse-grained $FeZn_{13}$ particles has a negative impact on the mechanical properties of the metal—dislocations pile up as they collide with the phase's interface, since sliding becomes more difficult, and the sample breaks down in brittle way, which was also confirmed in the study [23]. Likewise, the material's brittleness in the initial state is conditioned by the appearance of twins as one of the deformation mechanisms in HCP-lattice metals during tensile tests [24]. This phenomenon has also been demonstrated in the as-cast Zn-0.4%Mg and Zn-0.8%Mg alloys, where twins encountered each other and caused a local stress concentration leading to cracking [20]. Nevertheless, after a hot rolling treatment, the grains were refined, and deformation twinning was obstructed, hence the deformed samples had a better strength and ductility than the initial ones. The application of severe plastic deformation successfully solves the brittleness problem, which was reported in the study [25].

Investigation of corrosion properties, the results of which depend on the research method and the exposure time in a corrosive environment [26,27], has shown that the corrosion of zinc alloy is driven by the inhomogeneity in its chemical and phase composition [14,26–29]. Based on the results of the studies, it was established that the average corrosion rates for a coarse-grained and ultrafine-grained Zn-1%Mg-1%Fe alloy are equal to 0.05 mm/year and 0.061 mm/year, respectively [27,28]. The corrosion rates of the Zn-1%Fe-5%Mg alloy in its initial and HPT-treated states are 0.13 mm/year and 0.15 mm/year, respectively. The use of HPT treatment does not bring about sufficient changes in corrosion rates, but it does bring about more uniform corrosion throughout the sample (Figs. 4a,b).

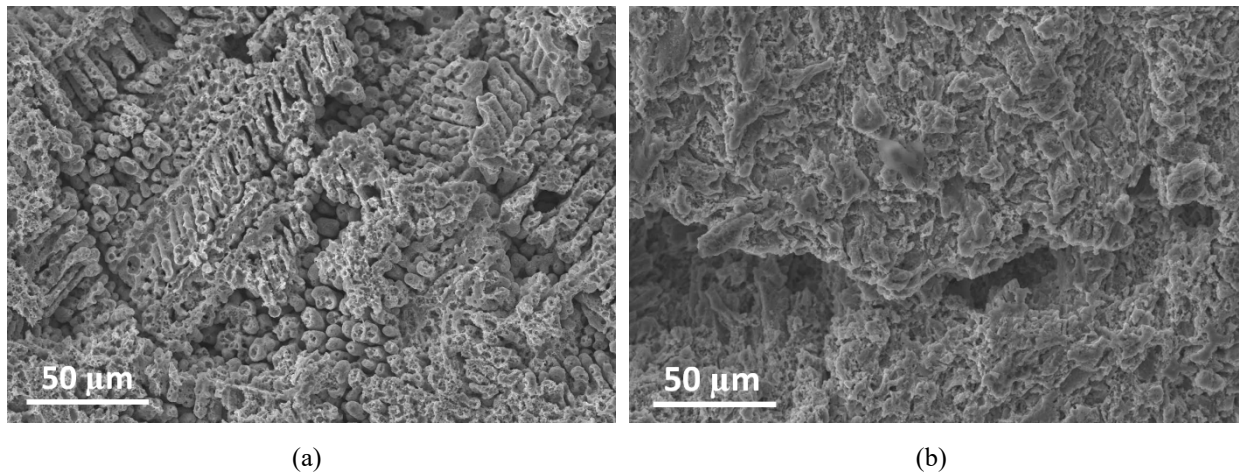


Fig. 4. Corrosion surface after 90 days of immersion tests of the Zn-1%Fe-5%Mg alloy: (a) initial state, (b) after HPT 10 revolutions.

In other studies of the corrosion behaviour of as-cast Zn- x Mg ($x = 1\%$, 2% , 3% , 5%) alloys, it was shown that the corrosion resistance of the alloy increased with the increase in magnesium content due to a protective film formed during the corrosion process [30]. However, in the case of the Zn-Fe-Mg alloy system, an increase in Mg content resulted in a 3...4-fold increase in corrosion rates, as the eutectics were subjected to corrosion so quickly that $Mg(OH)_2$ did not have sufficient time to deposit on the surface of the sample [31]. The major role in the acceleration of the corrosion processes was played by the microgalvanic effect between the Mg_2Zn_{11} and $FeZn_{13}$ phases, which arose due to the significant difference in the chemical potentials of Fe and Mg elements. The alloy with a higher Mg_2Zn_{11} volume fraction had a higher corrosion rate, i.e., Zn-1%Fe-5%Mg. Over time, zinc hydroxide was formed during the matrix corrosion, which slowed down the corrosion rate in the later stages of testing [14,28,29].

3.3. Morphological analysis

Results of morphological analysis showed that in wells with 25% and 12.5% extracts of Zn-1%Mg-1%Fe samples, only rounded cells without appendages or small, elongated cells were observed, the nuclei of which actively absorbed the dye propidium iodide, i.e., dead cells. Samples of extracts of Zn-1%Mg-5%Fe, which accounted for 25% of the volume of the medium, proved to be unfavorable for cells. The cells glowed brightly because of the fluorescence of propidium iodide in their nuclei. In wells with 12.5% extract of Zn-1%Mg-5%Fe samples, many attached, spread cells were noticed. They practically did not perceive the dye. The effect of contact inhibition and partial cell death were observed in wells with negative control as a result of their reaching a complete monolayer and depletion of the culture medium. In the wells of the positive

control with 25% and 12.5% dimethyl sulfoxide (DMSO), on the contrary, well-adhered cells were visible, occupying 40–60% of the surface of the well. Almost no dead cells were observed (Table 1).

However, despite the similar results of dying the cells MG63 with propidium iodide, there is a difference between the levels of cytotoxicity of the two alloys. After 7-day cellular testing the Zn-1%Fe-5%Mg alloy sample extracts exhibited the highest level of fluorescence, for the 12.5% extract level of fluorescence differed by up to 2.5 times (50% for the initial state of the Zn-1%Fe-5%Mg alloy, 45% for the HPT sample of the Zn-1%Fe-5%Mg alloy and 18% for Zn-1%Fe-1%Mg alloy). For the 25% extract, the values were on the same level of 20%. This indicates a higher number of surviving cells. The increase in Mg content leads to a rise in biocompatibility and promotes proliferation [32], as the Mg^{2+} ions have a beneficial effect on the formation of new cells.

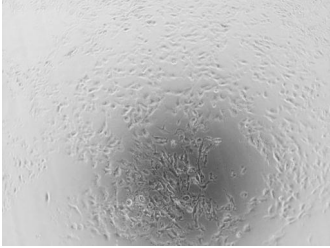
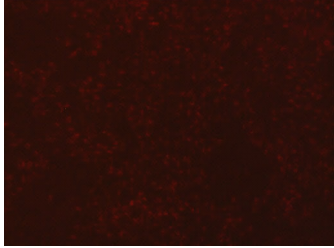
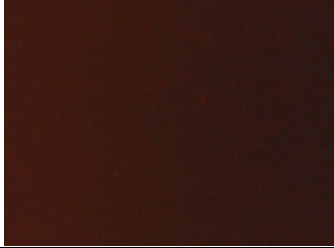
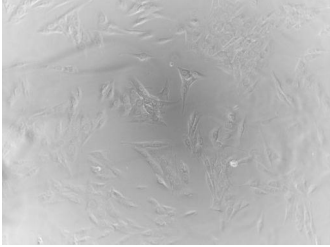
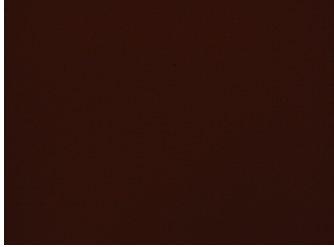
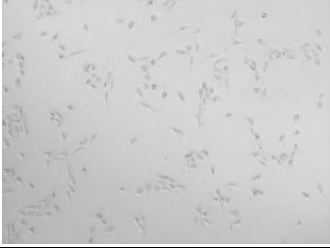
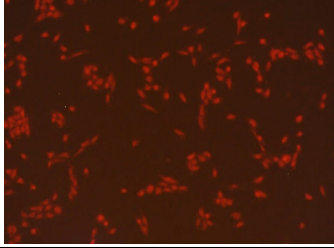
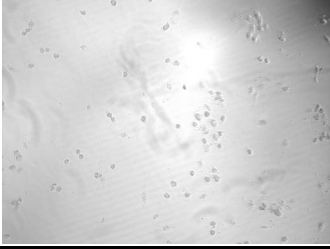
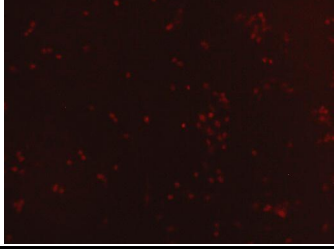
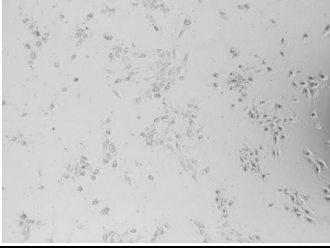
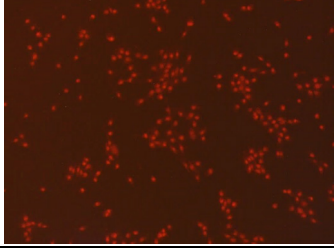
4. CONCLUSIONS

1. The increase in Mg content leads to inhomogeneity of structure caused by the formation of brittle intermetallics. Mg also enhances the strength of alloys due to solid-solution and dispersion strengthening, but high Mg content decreases ductility because of the brittleness of intermetallic phases.

2. The microstructures of the Zn-1%Fe-1%Mg and Zn-1%Fe-5%Mg alloys have a significant difference. In the alloy with 1 wt.% Mg, only the Mg_2Zn_{11} intermetallic phase is present, which localizes alongside the grain boundaries. With the increase in Mg content up to 5%, the additional phase occurs in the structure— $MgZn_2$ —forming the large particles over 150 microns in length.

3. Deformation treatment significantly raises the mechanical properties of the Zn-1%Fe-1%Mg alloy. Yield strength is up to 213 ± 12 MPa, UTS is up to 289 ± 11 MPa,

Table 1. Cell morphology after interaction with 25% and 12.5% extracts of Zn-1%Fe-1%Mg and Zn-1%Fe-5%Mg alloy after 10 revolutions of HPT.

	Sample	Phase contrast, x100	Propidium iodide, x100
	Negative control		
	Positive control DMSO 25%		
	Positive control DMSO 12.5%		
25%	Zn-1%Fe-1%Mg		
	Zn-1%Fe-5%Mg		
12.5%	Zn-1%Fe-1%Mg		
	Zn-1%Fe-5%Mg		

and the elongation is $95 \pm 5\%$. In the case of the Zn-1%Fe-5%Mg alloy, the high Mg content (5%) leads to a brittle fracture, which is not eliminated even after severe plastic deformation.

4. The addition of Mg contributes to an increase in the corrosion rate by 2.5 times in both initial and HPT samples. The corrosion rate of the HPT samples is higher in comparison to the initial ones.

5. In vitro tests demonstrated the absence of cytotoxic effects of extracts of the samples. The Zn-1%Fe-5%Mg alloy showed the greatest biological activity.

ACKNOWLEDGMENTS

The work was carried out at the expense of the academic leadership program of the Ufa University of Science and Technology (PRIORITY-2030). The research part of the work was carried out using the equipment of the Core Facility Centre “Nanotech” of Ufa University of Science and Technologies.

REFERENCES

- [1] A.M. Wu, C. Bisignano, S. James et al, Global, regional, and national burden of bone fractures in 204 countries and territories, 1990–2019: a systematic analysis from the Global Burden of Disease Study 2019, *The Lancet Healthy Longevity*, 2021, vol. 2, no. 9, pp. 580–592.
- [2] Z. Wang, Y. Zhang, J. Wu, Q. Zhang, Global, regional and country-specific burden of patella, tibia or fibula, or ankle fractures and its prediction to 2035: findings from global burden of disease study 2019, *BMC Public Health*, 2024, vol. 24, no. 1, art. no. 3162.
- [3] V.A. Samartsev, I.V. Kadyntsev, E.G. Voluzhenkov, Post-operative extremity metallosynthesis complications, *Perm Medical Journal*, 2018, vol. 35, no. 3, pp. 5–8.
- [4] X. Tong, X. Shen, Z. Lin, L. Lu, K. Munir, R. Zhou, L. Zhu, Y. Li, J. Ma, C. Wen, J. Lin, In vitro and in vivo studies of a biodegradable Zn-4Ag-0.1Sc alloy with high strength-elongation product, cytocompatibility, osteogenic differentiation, and anti-infection properties for guided bone-regeneration membrane applications, *Chemical Engineering Journal*, 2024, vol. 493, art. no. 152763.
- [5] X. Tong, Y. Han, L. Zhu, R. Zhou, Z. Lin, H. Wang, S. Huang, Y. Li, J. Ma, C. Wen, J. Lin, ZnP-Coated Zn-1Cu-0.1Ti Membrane with High Strength-Ductility, Antibacterial Ability, Cytocompatibility, and Osteogenesis for Biodegradable Guided Bone Regeneration Applications, *Advanced Functional Materials*, 2023, vol. 33, no. 31, art. no. 2214657.
- [6] T. Kraus, S.F. Fischerauer, A.C. Hänzli, P.J. Uggowitzer, J.F. Löffler, A.M. Weinberg, Magnesium alloys for temporary implants in osteosynthesis: In vivo studies of their degradation and interaction with bone, *Acta Biomaterialia*, 2012, vol. 8, no. 3, pp. 1230–1238.
- [7] D. Vojtěch, J. Kubásek, J. Čapek, Iva Pospíšilová Comparative mechanical and corrosion studies on magnesium, zinc and iron alloys as biodegradable metals, *Materials and Technology*, 2015, vol. 49, no. 6, pp. 877–882.
- [8] M.V. Polenok, E.D. Khafizova, R.K. Islamgaliev, The influence of severe plastic deformation on mechanical properties of pure zinc, *Frontier Materials & Technologies*, 2022, no. 3-2, pp. 25–31.
- [9] Y. Zheng, X. Xu, Z. Xu, J.Q. Wang, H. Cai, *Metallic Biomaterials: New Directions and Technologies*, Wiley-VCH Verlag GmbH & Co. KGaA, Weinheim, Germany, 2017.
- [10] H. Jin, L. Yang, L. Cui, L. Chen, Y. Lai, H. Guo, Y. Liu, Study on Properties of Zn-xMg (x=0.5, 0.8, 1) Alloys for Potential Stent Material, *Journal of Materials Engineering and Performance*, 2023, vol. 32, pp. 7468–7479.
- [11] J. Bai, Y. Xu, Q. Fan, R. Cao, X. Zhou, Z. Cheng, Q. Dong, F. Xue, Mechanical Properties and Degradation Behaviors of Zn-xMg Alloy Fine Wires for Biomedical Applications, *Scanning*, 2021, vol. 2021, no. 1, art. no. 4831387.
- [12] ISO 10993.5-99. *Medical products. Biological evaluation of medical devices — Part 5: Tests for in vitro cytotoxicity*, Standartinform Publ., Moscow, 2014, 10 p. (in Russian).
- [13] Z.Z. Shi, X.X. Gao, X.F. Liu, FeZn₁₃ intermetallic compound in biodegradable Zn-Fe alloy: Twinning and its shape effect, *Materials Characterization*, 2020, vol. 164, art. no. 110352.
- [14] E.D. Abdrakhmanova, E.D. Khafizova, M.V. Polenok, R.K. Nafikov, E.A. Korznikova, Influence of high-pressure torsion on the structure and mechanical properties of Zn-1%Fe-5%Mg zinc alloy, *Frontier Materials & Technologies*, 2024, no. 2, pp. 9–22.
- [15] V.D. Sitdikov, E.D. Khafizova, M.V. Polenok, Microstructure, crystallographic texture and mechanical properties of the Zn-1%Mg-1%Fe alloy subjected to severe plastic deformation, *Frontier Materials & Technologies*, 2024, no. 3, pp. 75–88.
- [16] Z.O. Králová, R. Gorejová, R. Oriňáková, M. Petráková, A. Oriňák, M. Kupková, M. Hrubovčáková, T. Sopčák, M. Baláž, I. Maskal'ová, A. Kovalčíková, K. Koval', Biodegradable zinc-iron alloys: Complex study of corrosion behavior, mechanical properties and hemocompatibility, *Progress in Natural Science: Materials International*, 2021, vol. 31, no. 2, pp. 279–287.
- [17] K. Han, I. Ohnuma, K. Okuda, R. Kainuma, Experimental determination of phase diagram in the Zn-Fe binary system, *Journal of Alloys and Compounds*, 2018, vol. 737, pp. 490–504.
- [18] C.Yao, Z. Wang, S.L. Tay, T. Zhu, W. Gao, Effects of Mg on microstructure and corrosion properties of Zn-Mg alloy, *Journal of Alloys and Compounds*, 2014, vol. 602, pp. 101–107.
- [19] T.A. Vida, T. Soares, R.S. Septimio, C.C. Brito, N. Cheung, A. Garcia, Effects of Macroseggregation and Microstructure on the Corrosion Resistance and Hardness of a Directionally Solidified Zn-5.0wt.%Mg Alloy, *Materials Research*, 2019, vol. 22.
- [20] S. Liu, D. Kent, N. Doan, M. Dargusch, G. Wang, Effects of deformation twinning on the mechanical properties of biodegradable Zn-Mg alloys, *Bioactive Materials*, 2018, vol. 4, pp. 8–16.
- [21] D.A. Porter, K.E. Easterling, M.Y. Sherif, *Phase Transformations in metals and alloys*, CRC Press, Boca Raton, 2009, 536 p.
- [22] Z.Z. Shi, X.X. Gao, H.T. Chen, X.F. Liu, A. Li, H.J. Zhang, L.N. Wang, Enhancement in mechanical and corrosion resistance properties of a biodegradable Zn-Fe alloy through second phase refinement, *Materials Science and Engineering: C*, 2020, vol. 116, art. no. 111197.

- [23] D. Lou, M. Zhang, J. Lv, B. Li, X. Wang, J. Shi, Y. Ren, H. Li, G. Qin, Effects of Fe addition on the microstructures and mechanical properties of as-extruded Zn-0.2Mg alloys, *Journal of Alloys and Compounds*, 2021, vol. 896, art. no. 162912.
- [24] M.H. Yoo, Slip, twinning, and fracture in hexagonal close-packed metals, *Metallurgical Transactions A*, 1981, vol. 12, pp. 409–418.
- [25] Z. Shi, C. Li, M. Li, X. Li, L. Wang, Second phase refining induced optimization of Fe alloying in Zn: Significantly enhanced strengthening effect and corrosion uniformity. *International Journal of Minerals, Metallurgy and Materials*, 2022, vol. 29, pp. 796–806.
- [26] E.D. Abdrakhmanova, E.D. Khafizova, M.V. Polenok, R.K. Islamgaliev, H. Yilmazer, Effect of the test regimes on the corrosion resistance of the Zn-1Fe-1Mg alloy. *Materials. Technologies. Design*, 2024, vol. 6, no. 1, pp. 80–90.
- [27] E.D. Abdrakhmanova, E.D. Khafizova, M.V. Polenok, V.D. Sitdikov, F.V. Nugamanov, Effect of exposure time in a physiological environment on the corrosion rate of ultrafine-grained Zn-Fe-Mg alloy, *Letters on Materials*, 2025, vol. 15, no. 1, pp. 60–65.
- [28] V.D. Sitdikov, E.D. Khafizova, M.V. Polenok, E.D. Abdrakhmanova, Corrosion resistance and biocompatibility of the ultrafine-grained Zn-1%Li-2%Mg and Zn-1.0%Mg-1.0%Fe alloys produced by severe plastic deformation, *Materials. Technologies. Design*, 2024, vol. 6, no. 2, pp. 109–128.
- [29] V.D. Sitdikov, E.D. Khafizova, M.V. Polenok, E.D. Abdrakhmanova, Corrosion resistance of ultrafine-grained Zn-1%Li-2%Mg and Zn-1.0%Mg-1.0%Fe alloys, *Russian Physics Journal*, 2024, vol. 67, pp. 2129–2135.
- [30] C. Yao, Z. Wang, S.L. Tay, T. Zhu, W. Gao, Effects of Mg on microstructure and corrosion properties of Zn–Mg alloy, *Journal of Alloys and Compounds*, 2014, vol. 602, pp. 101–107.
- [31] P. Xue, M. Ma, Y. Li, X. Li, J. Yuan, G. Shi, K. Wang, K. Zhang, Microstructure, Mechanical Properties, and in Vitro Corrosion Behavior of Biodegradable Zn-1Fe-xMg Alloy, *Materials*, 2020, vol. 13, no. 21, art. no. 4835.
- [32] N. Martynenko, N. Anisimova, O. Rybalchenko, M. Kiselevskiy, G. Rybalchenko, N. Tabachkova, M. Zheleznyi, D. Temralieva, V. Bazhenov, A. Koltygin, A. Sannikov, S. Dobatkin, Structure, Biodegradation, and In Vitro Bioactivity of Zn–1%Mg Alloy Strengthened by High-Pressure Torsion, *Materials*, 2022, vol. 15, no. 24, art. no. 9073.

УДК 691.75

Влияние содержания Mg на структуру, свойства и цитотоксичность биodeградируемых сплавов системы Zn-Fe-Mg

Э.Д. Абдрахманова^{1,2}, Э.Д. Хафизова¹, М.В. Поленок¹, Р.К. Исламгалиев¹, Zhen Li², Li Li², Yingru Liang², Meng Zhang²

¹ Уфимский университет науки и технологий, ул. Заки Валиди, д. 32, Уфа, 450076, Россия

² Harbin Engineering University, Nantong Str, No. 145, Harbin Heilongjiang, 150001, China

Аннотация. С каждым годом увеличивается интерес к биodeградируемым материалам для временных имплантатов на основе цинка. Цинковый сплав системы Zn-Fe-Mg представляет особый интерес, так как отдельно каждый элемент рассматривается как биodeградируемый металлический материал. В данной работе представлено всестороннее исследование свойств цинковых сплавов Zn-1%Fe-1%Mg и Zn-1%Fe-5%Mg, подвергнутых интенсивной пластической деформации кручением. Приведен сравнительный анализ структуры сплавов в литом состоянии и после деформации, отличия их фаз, свойств сплавов при одинаковой деформации, а также цитотоксичность материалов. Содержание Mg более 3 вес.% приводит к выделению дополнительной фазы MgZn₂, помимо уже присутствовавшей Mg₂Zn₁₁. Деформационная обработка сплава Zn-1%Fe-1%Mg способствует устранению его хрупкости и распределению эвтектики Mg₂Zn₁₁ равномерно по объему образца. Однако Zn-1%Fe-5%Mg обладает избыточной хрупкостью даже после деформации. Добавление Mg в сплав привело к ускорению коррозионных процессов. Механические, коррозионные, цитотоксичные свойства Zn-1%Fe-1%Mg соответствуют требованиям, предъявляемым к биodeградируемым материалам.

Ключевые слова: цинк; биodeградируемые материалы; коррозия; интенсивная пластическая деформация кручением; цитотоксичность